THE JOURNAL OF PHYSICAL CHEMISTRY C

Article

Cite This: J. Phys. Chem. C 2019, 123, 26735−26741

pubs.acs.org/JPCC

Hybrid Thermal Transport Characteristics of Doped Organic Semiconductor Poly(3,4-ethylenedioxythiophene):Tosylate

Xiaoxiang Yu,[†,‡] Ruiyang Li,[†,‡] Takuma Shiga,[§] Lei Feng,[§] Meng An,[∥] Lifa Zhang,[⊥] Junichiro Shiomi,*[,§,#] and Nuo Yang*[,†,‡]

[†]State Key Laboratory of Coal Combustion, Huazhong University of Science and Technology (HUST), Wuhan 430074, P. R. China

[‡]Nano Interface Center for Energy (NICE), School of Energy and Power Engineering, HUST, Wuhan 430074, P. R. China

[§]Department of Mechanical Engineering, The University of Tokyo, 7-3-1 Hongo, Bunkyo, Tokyo 113-8656, Japan

[∥]College of Mechanical and Electrical Engineering, Shaanxi University of Science and Technology, Xi'an 710021, P. R. China

[⊥]NNU-SULI Thermal Energy Research Center (NSTER) & Center for Quantum Transport and Thermal Energy Science (CQTES), School of Physics and Technology, Nanjing Normal University, Nanjing 210023, P. R. China

[#]Center for Materials Research by Information Integration, National Institute for Material Science, Tsukuba, Ibaraki 305-0047, Japan

Supporting Information

ABSTRACT: Understanding thermal transport in doped organic semiconductors would promote the development of flexible electronics and organic thermoelectrics. Temperature-dependent thermal conductivity of poly(3,4-ethylenedioxythiophene) (PEDOT) with different doping concentration is investigated by molecular dynamics simulations in a range of temperature from 200 to 400 K. The thermal conductivity of PEDOT is found to exhibit anisotropy and decrease with the doping concentration. The decomposition analysis of heat current reveals that doped PEDOT shows hybrid thermal transport characteristics including interfacial conduction between dopants and host polymers, lattice conduction in host polymers, and convection of dopants. For heavily-doped PEDOT at 400 K, convection can contribute up to 45% of the cross-plane total thermal conductivity, while host polymers remain in the solid state. The intensification of convection gives rise to positive temperature dependence of thermal conductivity in the cross-plane direction. Our study provides insight into the regulation of thermal transport in doped organic semiconductors.

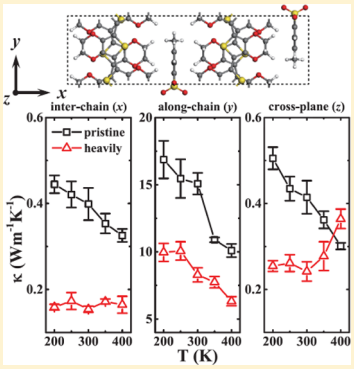

INTRODUCTION

Organic semiconductors have attracted extensive research interest recently as flexible semiconductors in wearable electronics, and energy-storage and conversion devices due to the advantages in high charge transport mobility, easy processing, mechanical flexibility, light weight, and low cost.[1−6] Poly(3,4-ethylenedioxythiophene) (PEDOT) is one of the most frequently studied conductive conjugated polymers for a wide range of utilization as organic optoelectronics,[7−11] biomedical applications,[12] organic electronics,[13−15] and organic thermoelectrics.[16−21] Among many kinds of properties concerned, thermal conductivity is of great importance for their applications. Low thermal conductivity is favorable to attain high energy conversion efficiency in thermoelectric elements, whereas excellent thermal transport is vital for heat dissipation in organic electronics and more sophisticated and integrated devices with high power density. With the development of energy conversion devices and increasing power density of electronics, there is a growing need to understand and modulate the heat transport in conjugated polymers such as PEDOT.

Many efforts have been devoted to exploring the thermal transport in pure polymer chains.[22−24] Zhang et al. reported the positive relationship between thermal conductivity of polymers and stiffness of backbone.[25] The thermal transport of polyethylene chains can be modulated by strain due to the morphology change.[26−28] Ma and Tian found that the introduction of side chain decreases the thermal conductivity of polymers.[29]

As well known, organic semiconductors (e.g., PEDOT) are indispensably doped to optimize their performance in real utilizations.[30−33] Therefore, investigating thermal transport of doped PEDOT is of practical significance. However, there are only a few works about the thermal properties of doped PEDOT. The dopants commonly used in PEDOT include poly(styrene sulfonate) (PSS), tosylate (Tos), and halides. Bubnova et al. obtained nearly isotropic thermal conductivity of spin-coated PEDOT:Tos using the 3ω technique.[34] By a differential 3ω method, Kim et al. demonstrated that engineered doping had an influence on the thermal anisotropy factor.[35] Liu et al. conducted time-domain thermoreflectance measurements and reported the highly anisotropic thermal conductivity of drop-casted PEDOT:PSS films with high electrical conductivity.[36] Wei et al. also observed the

Received: September 26, 2019
Revised: October 7, 2019
Published: October 8, 2019

DOI: 10.1021/acs.jpcc.9b09105
J. Phys. Chem. C 2019, 123, 26735−26741

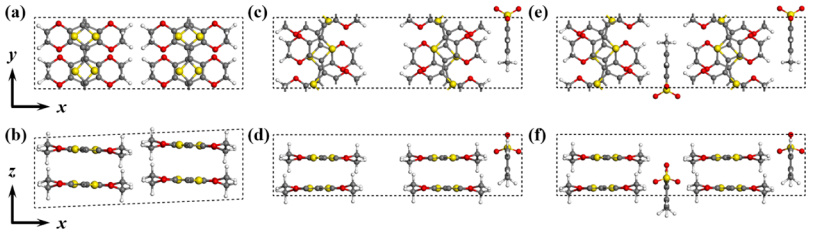

Figure 1. Schematic structures of (a,b) pristine, (c,d) lightly-, and (e,f) heavily-doped PEDOT crystals. The interchain, along-chain, and cross-plane direction are the *x*-, *y*-, and *z*-direction, respectively.

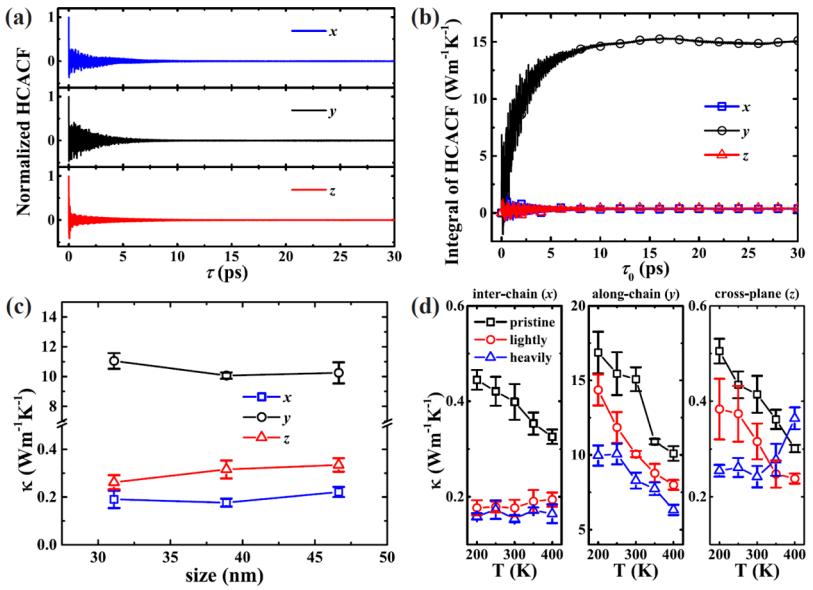

Figure 2. (a) The normalized heat flux auto-correlation function (HCACF) and (b) its integral of pristine PEDOT. (c) Dependence of thermal conductivity of lightly-doped PEDOT on the size of simulation cell. (d) Temperature dependence of thermal conductivity of PEDOT with different doping concentration.

anisotropic thermal conductivity by using flash analysis methods and attributed it to the oriented lamellar structure of PEDOT:PSS films.[37] Recently, through molecular dynamics (MD) simulations, Shi et al. reported the along-chain thermal conductivity values of PEDOT:Tos on the order of 10 $Wm^{-1}K^{-1}$.[38] Maeno et al.[39] and Crnjar et al.[40] investigated the along-chain thermal transport in PEDOT chains by MD simulations.

Yet, the effect of dopants on thermal transport has not attained enough attention. Some important issues such as thermal transport characteristics of doped PEDOT and influence of the dopants on the phonon properties of PEDOT are not answered. Such fundamental understanding is important because it not only assists in manipulating the thermal transport of PEDOT, but also offers guidelines for the optimization of doping strategies of organic thermoelectric materials.

In this work, we evaluate the doping effect on thermal transport in PEDOT and analyze the vibrational properties. Keeping in view that the electrical properties of doped PEDOT have been investigated enough, electronic thermal conductivity can be obtained from electric conductivity based on the widely-used Wiedemann−Franz law.[36] Hence, we do not consider the electronic thermal conductivity in this study. Compared with polyanions, small-sized anions such as Tos are easier to control their concentration and more convenient for atomistic simulations. Moreover, the dopants especially polyanions (e.g., PSS) may dramatically change the configurations of host polymers with a soft nature.[18,21] In reality, the polymer chains of conducting polymers are usually not well aligned.[18] Some experimental measurement works of PEDOT-based materials show different extent of anisotropy of thermal conductivities, indicating the uncertainty of material structures synthesized by different fabrication processes.[34−37] Therefore, as a base study, PEDOT:Tos crystal is preferred, due to the well-validated molecular structures and the convenience in comparison with previous simulation studies.[38,39] In addition, it is noteworthy that single-crystal PEDOT:Tos nanowires have been synthesized,[41] suggesting the promising potential of PEDOT:Tos. Experimental observations reported the doping level of PEDOT:Tos to be about one Tos molecule per four EDOT monomers.[42] Based on this, previous first-principles calculations showed the molecular structure of PEDOT:-Tos,[21,43] which is referred to as the heavily-doped one. Through artificially removing Tos molecules in the heavily-doped one, the lightly-doped PEDOT:Tos is obtained, whose doping level is reduced by half to one Tos molecule per eight EDOT monomers.[21] The structures of pristine, lightly-, and heavily-doped PEDOT crystals in ref 21 are used here. As depicted in Figure 1, Tos molecules are placed in the region between the PEDOT molecules in the *x*-direction.

METHODS

The MD simulation method is an effective way to obtain the thermal transport properties of materials with anharmonic-

DOI: 10.1021/acs.jpcc.9b09105
J. Phys. Chem. C 2019, 123, 26735−26741

ity.[44,45] To take the anharmonic vibrations into account, class II force field potential function including high-order terms and cross terms are widely applied to describe the interatomic bonded interactions depending on the structural components (bonds, angles, and dihedrals) and nonbonded interactions. For more accurate description of the interactions, the potential parameters of the sulfonic group in Tos are selected from improved force field parameters of sulfonate,[46] whereas the rest are from PCFF.[47] The equilibrium MD simulations were performed using the LAMMPS package[48] (see details in Section 1 of the Supporting Information). Green−Kubo formula relates the equilibrium fluctuations of heat current, in term of autocorrelation function, to thermal conductivity via the fluctuation−dissipation theorem. That is

$$\kappa_\alpha = \frac{1}{k_B T^2 V}\int_0^{\tau_0} \langle J_\alpha(0)\cdot J_\alpha(t)\rangle \mathrm{d}t$$

where α denotes the direction (x, y, and z), κ is the thermal conductivity, k_B is the Boltzmann constant, V is the system volume, T is the temperature, τ_0 is the integral upper limit, J is the heat current in the direction of interest, t is the correlation time, and the angular bracket denotes an ensemble average.[49] A combination of time and ensemble sampling is used to obtain better average statistics. The result represents the average of five independent simulations with different initial conditions.

RESULTS AND DISCUSSION

We evaluated the thermal transport in pristine, lightly-, and heavily-doped PEDOT crystals. As can be seen in Figure 2a, at 300 K, the heat current autocorrelation function (HCACF) curves of pristine PEDOT along the three directions decay within 10 picoseconds, and then fluctuate around zero. Figure 2b shows the integrals of HCACF along the x-, y-, and z-direction, which demonstrates the anisotropic thermal transport. Correspondingly, its integral converges to 0.35, 15.1, and 0.41 Wm^{-1} K^{-1} for the x-, y-, and z-direction, respectively. The HCACF and its integral of PEDOT crystals with different doping concentrations are shown in Figure S2. For pristine PEDOT, along-chain κ_y is much higher than the interchain κ_x and cross-plane κ_z. The anisotropic thermal transport is due to the strong covalent bonds along the chain but weak nonbonded interactions along the interchain and cross-plane directions. Moreover, κ_z is slightly larger than κ_x. The reason is that the intermolecular interactions along the stacking interactions between thiophene rings are stronger than those along the x-direction.[21,50]

The along-chain thermal conductivity (κ_y) is lower than that in previous MD results.[38,39] This discrepancy is attributed to different simulation method and force field. The equilibrium MD method is widely used to simulate the thermal transport of bulk materials.[51,52] To accurately simulate an infinite system with a finite simulation cell, periodic boundary conditions are applied along the three directions. Because vibrational modes with wavelength longer than the simulation cell length cannot be considered, the convergence of thermal conductivity with respect to the cell size was confirmed as shown in Figure 2c. Therefore, the equilibrium MD allows us to simulate the infinite size, that is, bulk thermal conductivity, which is different from nonequilibrium MD method that is suited to study the size dependence of thermal conductivity, for instance, in nanomaterials.[53−57] Note that nonequilibrium MD simulations have also been used to study bulk thermal conductivity by extrapolating the values calculated for various sizes. Previous research showed that the thermal conductivity values estimated by nonequilibrium MD for nanowires and polymer chains are typically higher than those by equilibrium MD method.[28,58,59] In addition, the previous nonequilibrium MD simulations by Shi et al.[38] and Maeno et al.[39] employed class I force field including only quadratic terms for bonds and angles, whereas class II force field including high-order terms for bonds and angles is used in this work. High-order terms in class II force field make atomic vibrations more anharmonic compared with quadratic terms in class I force field, so the thermal conductivity obtained from class II force field is expected to be lower.[25] In general, our value also falls into the value range of thermal conductivity of analogous conjugated polymers calculated using the same class II force field.[25]

Next, we investigated the temperature dependence of thermal conductivity. As shown in Figure 2d, for pristine PEDOT, thermal conductivity along the three directions exhibits typical negative temperature dependence. Additionally, along-chain thermal conductivity for doped PEDOT also shows a decreasing trend. On the other hand, there exist some anomalous thermal transport behaviors for doped PEDOT with Tos molecules. For the interchain direction, κ_x of lightly- and heavily-doped PEDOT (0.18 and 0.15 Wm^{-1} K^{-1} at 300 K, respectively) is lower than that of the pristine one (0.35 Wm^{-1} K^{-1} at 300 K). Intuitively, the Tos molecules located between two PEDOT chains along the x-direction should be responsible for the deteriorative interchain heat propagation. Both PEDOT and Tos are planar conjugated molecules, but form perpendicular arrangement. Wang et al. found a temperature discontinuity between two planar DNTT conjugated molecular crystals along different orientation of molecular plane, and reported strong phonon scattering and large Kapitza resistance in interface regions.[60] Similarly, PEDOT and Tos molecules with different plane orientation generate thermal interfaces and significantly reduce thermal conductivity along the x-direction. The slightly lower κ_x of heavily-doped PEDOT arises from higher doping concentration and thus larger volume density of interface regions compared with lightly-doped PEDOT. Correspondingly, there is no obvious temperature dependence of κ_x, which is similar to previous results about thermal interfaces.[61−63]

For the cross-plane direction, the room-temperature κ_z values for pristine, lightly-, and heavily-doped PEDOT are 0.41, 0.32, and 0.24 Wm^{-1} K^{-1}, respectively. As for the temperature dependence, κ_z of heavily-doped PEDOT exhibits positive dependence, in contrast to the pristine and lightly-doped ones that show the negative dependence. When considering the contribution to heat transfer, there is only one channel in pristine PEDOT along the z-direction, namely, interlayer heat conduction. However, for doped PEDOT, another additional channel is the intermolecular heat transfer by Tos molecules between PEDOT. The anomalous temperature dependence of κ_z of heavily-doped PEDOT is attributed to the competing contribution of PEDOT and Tos molecules, resulting from different heat transport characteristics as will be discussed later.

The room-temperature along-chain thermal conductivity decreases from 15.1 Wm^{-1} K^{-1} for pristine PEDOT to 10.1 and 8.3 Wm^{-1} K^{-1} for lightly- and heavily-doped structures, respectively. As the addition of Tos molecules alters the volume of the simulation system, we calculated the cross-

DOI: 10.1021/acs.jpcc.9b09105
J. Phys. Chem. C 2019, 123, 26735−26741

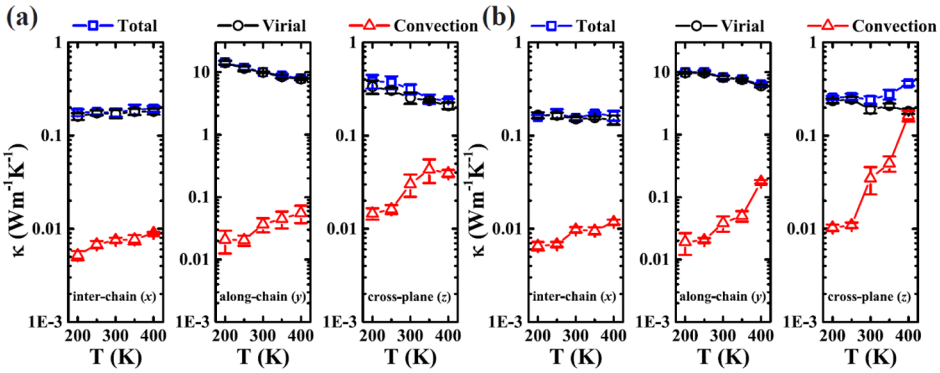

Figure 3. Contribution of virial and convection terms to temperature-dependent thermal conductivity of (a) lightly- and (b) heavily-doped PEDOT.

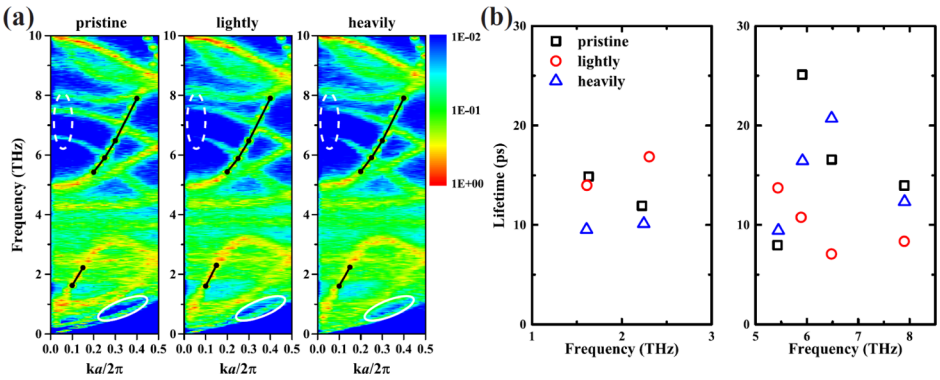

Figure 4. (a) Along-chain SED maps of pristine, lightly-, and heavily-doped PEDOT at room temperature. Normalized wave vector $ka/2\pi$ is used due to the negligible differences of *y*-direction lattice constant shown in Table S2. The white dashed ellipses denote the gradual attenuation of SED spectra of doped PEDOT in comparison with pristine PEDOT. The white solid ellipses point out the decreasing area of blue region with increasing doping concentration. The black solid lines indicate the selected phonon modes with Lorentzian-shape peaks. (b) Lifetimes of phonon modes denoted by dots on black solid lines in (a).

sectional area of the *xz*-plane at 300 K for pristine, lightly-, and heavily-doped PEDOT crystals, as shown in Table S2. Obviously, PEDOT dominates heat transport in the along-chain direction. Provided that the Tos molecules have no contribution to heat transport in the *y*-direction, the occupied area of Tos molecules is deleted to make the comparison of κ_y legitimately. Hence, the modified κ_y values of PEDOT are recalculated as 12.2 and 11.6 Wm^{-1} K^{-1} for lightly- and heavily-doped PEDOT, respectively. As can be seen, there still exists an approximate 1/5 reduction of thermal conductivity. It is intuitive to ascribe the thermal conductivity suppression to the phonon scattering induced by dopant−PEDOT interactions. Further analysis will be shown later. The negative temperature dependence of κ_y is consistent with those of other typical polymer crystals.[24,27] This is due to the increased phonon scattering with increasing temperature as discussed in Figure S3. As Figure S4 shows, the morphology characterization of PEDOT chains via the radial distribution function indicates that phase change is not the reason for the reduction in along-chain thermal conductivity.

To quantitatively analyze the thermal transport characteristics in doped PEDOT, we decompose the total thermal conductivity into contributions from different mechanisms. The heat current is calculated as

$$J = \sum_{i=1}^{N} e_i v_i + \frac{1}{2}\sum_{i=1}^{N}\sum_{j=1;j\neq i}^{N} (F_{ij}\cdot v_i) r_{ij}$$

where e_i and v_i are the energy and velocity of atom *i*, and F_{ij} and r_{ij} are force and position vectors between atoms *i* and *j*, respectively. The contribution of convection and virial to heat current correspond to the first and second term, respectively. Usually, virial contribution to thermal transport is dominant owing to the weak atomic convectional motion.[64] However, because of the presence of small-sized Tos anions, convection would make certain contribution to thermal conductivity in doped PEDOT. The total thermal conductivity can be decomposed into three contributions, convection ($\kappa_{convection}$), virial (κ_{virial}), and the coupling between virial and convection, denoted as κ_{cross}. Commonly, κ_{cross} is very small, and presents the same temperature dependence as $\kappa_{convection}$.[64] As will be seen in Figure 3, the sum of $\kappa_{convection}$ and κ_{virial} is close to κ_{total}, so we do not discuss the value of κ_{cross} here.

Figure 3a shows the virial and convectional contribution to thermal conductivity of lightly-doped PEDOT at different temperatures. For thermal conductivity along the three directions, κ_{virial} overwhelms thermal transport and is higher than $\kappa_{convection}$ by more than one order of magnitude. Thermal transport in the *x*-direction is governed by the interfacial thermal conduction as mentioned above, and there is no obvious temperature dependence of κ_{virial}. In the *y*- and *z*-direction, κ_{virial} shows conventional negative temperature dependence. $\kappa_{convection}$ increases as temperature increases due to the intensification of convection. $\kappa_{convection}$ in the *y*- and *z*-direction are comparable and are higher than $\kappa_{convection}$ in the *x*-direction because of the anisotropic motion of Tos molecules.

DOI: 10.1021/acs.jpcc.9b09105
J. Phys. Chem. C 2019, 123, 26735−26741

The mean square displacement (MSD) calculation in Figure S5c,d demonstrates larger MSD values in the *y*- and *z*-direction compared with that in the *x*-direction. This means that the motion of Tos molecules is unrestricted in the *y*- and *z*-direction, whereas it is restricted by PEDOT in the *x*-direction. As can be seen in Figure 3b, compared with lightly-doped PEDOT, heavily-doped PEDOT shows similar results in the *x*-direction. However, $\kappa_{convection}$ in the *y*- and *z*-direction of heavily-doped PEDOT are much larger than those of the lightly-doped one. Especially, at 400 K, $\kappa_{convection}$ reaches 45% of the total thermal conductivity, becoming comparable to κ_{virial} in the *z*-direction. The abnormally positive temperature dependence of thermal conductivity in the *z*-direction results from the huge increase of $\kappa_{convection}$. Figure S5a,b shows solid-like converging and fluctuating MSD of PEDOT with running time, which denotes that PEDOT remains in the solid state. Morphology characterization in Figure S4 also verifies no phase change for PEDOT. For Tos molecules, Figure S5d demonstrates that the MSD of Tos molecules keep increasing with running time. The linear increasing trend is confirmed in Figure S6a and Table S3. The diffusion coefficient calculation in Figure S6b predicts the liquid-like diffusion characteristics of Tos molecules in heavily-doped PEDOT at 400 K,[64] and thus proves the considerable contribution from convection of Tos molecules. Therefore, the system is partial-solid partial-liquid at 400 K, which means that the Tos molecules diffuse like liquid in the gaps between solid PEDOT.

To gain further understanding of the doping effect on κ_{virial}, the normalized spectral energy density (SED) is calculated to qualitatively analyze the difference in along-chain heat conduction. Through Lorentzian function fitting, the phonon lifetimes of pristine, lightly-, and heavily-doped PEDOTs can be obtained.[54,65−67] The along-chain SED in the full-frequency range is given in Figure S7a. Keeping in view that dominant thermal energy carriers in crystalline polymers are usually low-frequency phonons,[68] an enlarged SED contour map in the frequency range below 10 THz is presented in Figure 4a. As denoted by white dashed ellipses, along the direction from the Brillouin zone edge to the center, these optical branches of pristine PEDOT exhibit clear spectra, whereas those of doped PEDOT show gradual attenuation. Additionally, the area of the blue region in the white solid ellipse gradually decreases with the increasing doping concentration. These two phenomena indicate the generally broader SED peaks and smaller phonon lifetimes of doped PEDOT in comparison with the pristine one. Besides, the phonon branches of pristine PEDOT above the white solid ellipses are clearer than those of doped ones, whereas those of lightly-doped PEDOT are clearer than those of the heavily-doped one, suggesting steeper SED peaks, and thus larger phonon lifetimes of pristine PEDOT.[69]

The quantification of lifetimes for all phonon modes of PEDOT would be highly time-consuming due to the numerous branches in the first Brillouin zone. Here, to partly exemplify the reduction of phonon lifetimes, the SED spectra are fitted by Lorentzian functions for several phonon modes with Lorentzian-shape peaks. According to the SED spectra of PEDOT shown in Figure S8, as denoted by dots on black solid lines in Figure 4a, two acoustic phonon modes with normalized wave number from 0.1 to 0.15 and four optical phonon modes with normalized wave number from 0.2 to 0.4 are selected. These phonon modes have large slopes (i.e., large group velocities), hence considerable contributions to thermal transport. As Figure 4b shows, lifetimes of not all but most phonon modes in pristine PEDOT are larger than those of doped ones, which is consistent with the nonsignificant difference between modified κ_y. When roughly considering only these phonon modes, lifetimes exhibit general decreasing trend from pristine PEDOT to doped ones, whereas phonon lifetimes of lightly- and heavily-doped PEDOT are close. The general reduction of phonon lifetimes in the low-frequency range validates the decreased along-chain thermal conductivity of PEDOT by doping.

In the high-frequency range, the discrepancy between SED of pristine, lightly-, and heavily-doped PEDOT are not obvious. As depicted in Figure S9, the enlarged plot in the frequency range of 40−50 THz shows similar SED contour maps. In other words, dopants mainly suppress the heat transport via low-frequency phonons because the interactions between dopants and host polymers are nonbonded forces, which mainly affect low-frequency atomic vibrations.

CONCLUSIONS

In conclusion, we have performed MD simulations of the thermal transport in pristine, lightly-, and heavily-doped PEDOT. The temperature dependent thermal conductivity from 200 to 400 K demonstrates the anisotropic thermal transport in PEDOT. Furthermore, it is found that doping decreases the thermal conductivity of PEDOT along the three directions at room temperature. Pristine PEDOT presents conventional negative temperature-dependent thermal conductivity. For doped PEDOT, along-chain thermal conductivity shows negative temperature dependence, whereas cross-plane thermal conductivity exhibits a positive trend. There is no obvious temperature dependence of interchain thermal conductivity due to the interface-like nature of thermal transport between PEDOT and dopants. Through the quantitative analysis of the respective contribution to thermal conductivity of doped PEDOT from virial and convection, it is disclosed that $\kappa_{convection}$ increases with temperature due to the intensification of convection. Especially, convection can contribute up to 45% of the cross-plane total thermal conductivity of heavily-doped PEDOT at 400 K. The analysis of morphology and diffusion confirm the system state as partial-solid partial-liquid at 400 K, which means that Tos molecules diffuse like liquid in the gaps between solid PEDOT. Moreover, along-chain and cross-plane κ_{virial} decreases with temperature. The SED analysis shows the general decrease of phonon lifetimes in low-frequency range, indicating that doping mainly affects low-frequency phonons due to the nonbonded interactions between Tos and PEDOT. The addition of dopants results in both volume change and phonon scattering, thus reducing the thermal conductivity in the *y*-direction. The result demonstrates the hybrid thermal transport characteristics in doped PEDOT. Our study provides insights into the thermal transport mechanism in doped organic semiconductors and guides the regulation of thermal properties for their applications in electronic devices and energy conversion.

ASSOCIATED CONTENT

Supporting Information

The Supporting Information is available free of charge on the ACS Publications website at DOI: 10.1021/acs.jpcc.9b09105.

Simulation details and additional results including two tables about simulation settings and structure parame-

DOI: 10.1021/acs.jpcc.9b09105
J. Phys. Chem. C 2019, 123, 26735−26741

ters, simulation system parameters during relaxation process, HCACF and the integrals, vibrational density of states, radial distribution function, MSD and diffusion coefficient, and SED (PDF)

AUTHOR INFORMATION

Corresponding Authors

*E-mail: shiomi@photon.t.u-tokyo.ac.jp (J.S.).
*E-mail: nuo@hust.edu.cn (N.Y.).

ORCID

Xiaoxiang Yu: 0000-0001-8072-6773
Takuma Shiga: 0000-0002-5103-7853
Meng An: 0000-0002-1560-7329
Lifa Zhang: 0000-0001-6108-1404
Junichiro Shiomi: 0000-0002-3552-4555
Nuo Yang: 0000-0003-0973-1718

Notes

The authors declare no competing financial interest.

ACKNOWLEDGMENTS

N.Y. is supported by National Natural Science Foundation of China (nos. 51576076 and 51711540031), Natural Science Foundation of Hubei Province (2017CFA046), and Fundamental Research Funds for the Central Universities (HUST, 2019kfyRCPY045). The authors thank the National Supercomputing Center in Tianjin (TianHe-1 (A)) and China Scientific Computing Grid (ScGrid) for providing assistance in computations. J.S. is supported in part by Bilateral Joint Research Project and KAKENHI grant no. 19H00744 by JSPS. The authors acknowledge useful discussions with Wen Shi, Zhigang Shuai, and Yinhua Zhou.

REFERENCES

(1) Xie, K.; Wei, B. Materials and Structures for Stretchable Energy Storage and Conversion Devices. *Adv. Mater.* **2014**, *26*, 3592−3617.
(2) Xu, J.; Wang, S. H.; Wang, G. J. N.; Zhu, C. X.; Luo, S. C.; Jin, L. H.; Gu, X. D.; Chen, S. C.; Feig, V. R.; To, J. W. F.; et al. Highly Stretchable Polymer Semiconductor Films through the Nanoconfinement Effect. *Science* **2017**, *355*, 59−64.
(3) Lei, T.; Guan, M.; Liu, J.; Lin, H.-C.; Pfattner, R.; Shaw, L.; McGuire, A. F.; Huang, T.-C.; Shao, L.; Cheng, K.-T.; et al. Biocompatible and Totally Disintegrable Semiconducting Polymer for Ultrathin and Ultralightweight Transient Electronics. *Proc. Natl. Acad. Sci. U.S.A.* **2017**, *114*, 5107−5112.
(4) Mi, X.-Y.; Yu, X.; Yao, K.-L.; Huang, X.; Yang, N.; Lü, J.-T. Enhancing the Thermoelectric Figure of Merit by Low-Dimensional Electrical Transport in Phonon-Glass Crystals. *Nano Lett.* **2015**, *15*, 5229−5234.
(5) Bubnova, O.; Crispin, X. Towards Polymer-Based Organic Thermoelectric Generators. *Energy Environ. Sci.* **2012**, *5*, 9345−9362.
(6) Amanchukwu, C. V.; Gauthier, M.; Batcho, T. P.; Symister, C.; Shao-Horn, Y.; D'Arcy, J. M.; Hammond, P. T. Evaluation and Stability of PEDOT Polymer Electrodes for Li−O_2 Batteries. *J. Phys. Chem. Lett.* **2016**, *7*, 3770−3775.
(7) Qiao, W.; Huang, W.; Liu, Y.; Li, X.; Chen, L.-S.; Tang, J.-X. Toward Scalable Flexible Nanomanufacturing for Photonic Structures and Devices. *Adv. Mater.* **2016**, *28*, 10353−10380.
(8) Cai, Y.; Huo, L.; Sun, Y. Recent Advances in Wide-Bandgap Photovoltaic Polymers. *Adv. Mater.* **2017**, *29*, 1605437.
(9) Thomas, J. P.; Rahman, M. A.; Srivastava, S.; Kang, J.-S.; McGillivray, D.; Abd-Ellah, M.; Heinig, N. F.; Leung, K. T. Highly Conducting Hybrid Silver-Nanowire-Embedded Poly(3,4-Ethylenedioxythiophene):Poly(Styrenesulfonate) for High-Efficiency Planar Silicon/Organic Heterojunction Solar Cells. *ACS Nano* **2018**, *12*, 9495−9503.
(10) Liu, J.; Pathak, S.; Stergiopoulos, T.; Leijtens, T.; Wojciechowski, K.; Schumann, S.; Kausch-Busies, N.; Snaith, H. J. Employing PEDOT as the p-Type Charge Collection Layer in Regular Organic−Inorganic Perovskite Solar Cells. *J. Phys. Chem. Lett.* **2015**, *6*, 1666−1673.
(11) Hu, L.; Li, M.; Yang, K.; Xiong, Z.; Yang, B.; Wang, M.; Tang, X.; Zang, Z.; Liu, X.; Li, B.; et al. PEDOT:PSS Monolayers to Enhance the Hole Extraction and Stability of Perovskite Solar Cells. *J. Mater. Chem. A* **2018**, *6*, 16583−16589.
(12) Luo, S.-C. Conducting Polymers as Biointerfaces and Biomaterials: A Perspective for a Special Issue of Polymer Reviews. *Polym. Rev.* **2013**, *53*, 303−310.
(13) Wang, Y.; Zhu, C.; Pfattner, R.; Yan, H.; Jin, L.; Chen, S.; Molina-Lopez, F.; Lissel, F.; Liu, J.; Rabiah, N. I.; et al. A Highly Stretchable, Transparent, and Conductive Polymer. *Sci. Adv.* **2017**, *3*, No. e1602076.
(14) Zhou, Y.; Fuentes-Hernandez, C.; Shim, J.; Meyer, J.; Giordano, A. J.; Li, H.; Winget, P.; Papadopoulos, T.; Cheun, H.; Kim, J. A Universal Method to Produce Low−Work Function Electrodes for Organic Electronics. *Science* **2012**, *336*, 327−332.
(15) Lu, B.; Yuk, H.; Lin, S.; Jian, N.; Qu, K.; Xu, J.; Zhao, X. Pure PEDOT:PSS Hydrogels. *Nat. Commun.* **2019**, *10*, 1043.
(16) Lee, D.; Sayed, S. Y.; Lee, S.; Kuryak, C. A.; Zhou, J.; Chen, G.; Shao-Horn, Y. Quantitative Analyses of Enhanced Thermoelectric Properties of Modulation-Doped PEDOT:PSS/Undoped Si (001) Nanoscale Heterostructures. *Nanoscale* **2016**, *8*, 19754−19760.
(17) Russ, B.; Glaudell, A.; Urban, J. J.; Chabinyc, M. L.; Segalman, R. A. Organic Thermoelectric Materials for Energy Harvesting and Temperature Control. *Nat. Rev. Mater.* **2016**, *1*, 16050.
(18) Wei, Q.; Mukaida, M.; Kirihara, K.; Naitoh, Y.; Ishida, T. Recent Progress on PEDOT-Based Thermoelectric Materials. *Materials* **2015**, *8*, 732−750.
(19) Yao, H.; Fan, Z.; Li, P.; Li, B.; Guan, X.; Du, D.; Ouyang, J. Solution Processed Intrinsically Conductive Polymer Films with High Thermoelectric Properties and Good Air Stability. *J. Mater. Chem. A* **2018**, *6*, 24496−24502.
(20) Guan, X.; Cheng, H.; Ouyang, J. Significant Enhancement in the Seebeck Coefficient and Power Factor of Thermoelectric Polymers by the Soret Effect of Polyelectrolytes. *J. Mater. Chem. A* **2018**, *6*, 19347−19352.
(21) Shi, W.; Zhao, T.; Xi, J.; Wang, D.; Shuai, Z. Unravelling Doping Effects on PEDOT at the Molecular Level: From Geometry to Thermoelectric Transport Properties. *J. Am. Chem. Soc.* **2015**, *137*, 12929−12938.
(22) Xu, X.; Chen, J.; Zhou, J.; Li, B. Thermal Conductivity of Polymers and Their Nanocomposites. *Adv. Mater.* **2018**, *30*, 1705544.
(23) Huang, C.; Qian, X.; Yang, R. Thermal Conductivity of Polymers and Polymer Nanocomposites. *Mater. Sci. Eng., R* **2018**, *132*, 1−22.
(24) Meng, H.; Yu, X.; Feng, H.; Xue, Z.; Yang, N. Superior Thermal Conductivity of Poly (Ethylene Oxide) for Solid-State Electrolytes: A Molecular Dynamics Study. *Int. J. Heat Mass Transfer* **2019**, *137*, 1241−1246.
(25) Zhang, T.; Wu, X.; Luo, T. Polymer Nanofibers with Outstanding Thermal Conductivity and Thermal Stability: Fundamental Linkage between Molecular Characteristics and Macroscopic Thermal Properties. *J. Phys. Chem. C* **2014**, *118*, 21148−21159.
(26) Liu, J.; Yang, R. G. Tuning the Thermal Conductivity of Polymers with Mechanical Strains. *Phys. Rev. B: Condens. Matter Mater. Phys.* **2010**, *81*, 174122.
(27) Zhang, T.; Luo, T. Morphology-Influenced Thermal Conductivity of Polyethylene Single Chains and Crystalline Fibers. *J. Appl. Phys.* **2012**, *112*, 094304.
(28) He, J.; Kim, K.; Wang, Y.; Liu, J. Strain Effects on the Anisotropic Thermal Transport in Crystalline Polyethylene. *Appl. Phys. Lett.* **2018**, *112*, 051907.

DOI: 10.1021/acs.jpcc.9b09105
J. Phys. Chem. C 2019, 123, 26735−26741

(29) Ma, H.; Tian, Z. Effects of Polymer Topology and Morphology on Thermal Transport: A Molecular Dynamics Study of Bottlebrush Polymers. *Appl. Phys. Lett.* **2017**, *110*, 091903.
(30) Al Attar, H. A.; Monkman, A. P. Dopant Effect on the Charge Injection, Transport, and Device Efficiency of an Electrophosphorescent Polymeric Light-Emitting Device. *Adv. Funct. Mater.* **2006**, *16*, 2231−2242.
(31) Liu, C.; Jang, J.; Xu, Y.; Kim, H. J.; Khim, D.; Park, W. T.; Noh, Y. Y.; Kim, J. J. Effect of Doping Concentration on Microstructure of Conjugated Polymers and Characteristics in n-Type Polymer Field-Effect Transistors. *Adv. Funct. Mater.* **2015**, *25*, 758−767.
(32) Huang, J. S.; Miller, P. F.; Wilson, J. S.; de Mello, A. J.; de Mello, J. C.; Bradley, D. D. C. Investigation of the Effects of Doping and Post-Deposition Treatments on the Conductivity, Morphology, and Work Function of Poly (3,4-Ethylenedioxythiophene)/Poly (Styrene Sulfonate) Films. *Adv. Funct. Mater.* **2005**, *15*, 290−296.
(33) He, F.; Cheng, C.; Geng, H.; Yi, Y.; Shuai, Z. Effect of Donor Length on Electronic Structures and Charge Transport Polarity for DTDPP-Based D-A Copolymers: A Computational Study Based on a Super-Exchange Model. *J. Mater. Chem. A* **2018**, *6*, 11985−11993.
(34) Bubnova, O.; Khan, Z. U.; Malti, A.; Braun, S.; Fahlman, M.; Berggren, M.; Crispin, X. Optimization of the Thermoelectric Figure of Merit in the Conducting Polymer Poly(3,4-Ethylenedioxythiophene). *Nat. Mater.* **2011**, *10*, 429−433.
(35) Kim, G.-H.; Shao, L.; Zhang, K.; Pipe, K. P. Engineered Doping of Organic Semiconductors for Enhanced Thermoelectric Efficiency. *Nat. Mater.* **2013**, *12*, 719−723.
(36) Liu, J.; Wang, X. J.; Li, D. Y.; Coates, N. E.; Segalman, R. A.; Cahill, D. G. Thermal Conductivity and Elastic Constants of PEDOT:PSS with High Electrical Conductivity. *Macromolecules* **2015**, *48*, 585−591.
(37) Wei, Q.; Mukaida, M.; Kirihara, K.; Ishida, T. Experimental Studies on the Anisotropic Thermoelectric Properties of Conducting Polymer Films. *ACS Macro Lett.* **2014**, *3*, 948−952.
(38) Shi, W.; Shuai, Z.; Wang, D. Tuning Thermal Transport in Chain-Oriented Conducting Polymers for Enhanced Thermoelectric Efficiency: A Computational Study. *Adv. Funct. Mater.* **2017**, *27*, 1702847.
(39) Maeno, S.; Cannon, J. J.; Shiga, T.; Shiomi, J. Molecular Dynamics Study on Heat Conduction in Poly(3,4-Ethylenedioxythiophene). *Jpn. J. Appl. Phys.* **2018**, *57*, 101601.
(40) Crnjar, A.; Melis, C.; Colombo, L. Assessing the Anomalous Superdiffusive Heat Transport in a Single One-Dimensional PEDOT Chain. *Phys. Rev. Mater.* **2018**, *2*, 015603.
(41) Cho, B.; Park, K. S.; Baek, J.; Oh, H. S.; Koo Lee, Y. E.; Sung, M. M. Single-Crystal Poly(3,4-Ethylenedioxythiophene) Nanowires with Ultrahigh Conductivity. *Nano Lett.* **2014**, *14*, 3321−3327.
(42) Aasmundtveit, K. E.; Samuelsen, E. J.; Pettersson, L. A. A.; Inganas, O.; Johansson, T.; Feidenhans, R. Structure of Thin Films of Poly(3,4-Ethylenedioxythiophene). *Synth. Met.* **1999**, *101*, 561−564.
(43) Kim, E.-G.; Brédas, J.-L. Electronic Evolution of Poly(3,4-Ethylenedioxythiophene) (PEDOT): From the Isolated Chain to the Pristine and Heavily Doped Crystals. *J. Am. Chem. Soc.* **2008**, *130*, 16880−16889.
(44) Hu, S.; An, M.; Yang, N.; Li, B. A Series Circuit of Thermal Rectifiers: An Effective Way to Enhance Rectification Ratio. *Small* **2017**, *13*, 1602726.
(45) Li, S.; Yu, X.; Bao, H.; Yang, N. High Thermal Conductivity of Bulk Epoxy Resin by Bottom-Up Parallel-Linking and Strain: A Molecular Dynamics Study. *J. Phys. Chem. C* **2018**, *122*, 13140−13147.
(46) Huige, C. J. M.; Altona, C. Force-Field Parameters for Sulfates and Sulfamates Based on Ab Initio Calculations: Eextensions of AMBER and CHARMm Fields. *J. Comput. Chem.* **1995**, *16*, 56−79.
(47) Sun, H.; Mumby, S. J.; Maple, J. R.; Hagler, A. T. An ab Initio CFF93 All-Atom Force Field for Polycarbonates. *J. Am. Chem. Soc.* **1994**, *116*, 2978−2987.
(48) Plimpton, S. Fast Parallel Algorithms for Short-Range Molecular Dynamics. *J. Comput. Phys.* **1995**, *117*, 1−19.
(49) Kang, J.; Wang, L.-W. First-principles Green-Kubo method for thermal conductivity calculations. *Phys. Rev. B* **2017**, *96*, No. 020302(R).
(50) Ding, Z.; An, M.; Mo, S.; Yu, X.; Jin, Z.; Liao, Y.; Esfarjani, K.; Lü, J.-T.; Shiomi, J.; Yang, N. Unexpectedly High Cross-Plane Thermoelectric Performance of Layered Carbon Nitrides. *J. Mater. Chem. A* **2019**, *7*, 2114−2121.
(51) Ma, D.; Ding, H.; Meng, H.; Feng, L.; Wu, Y.; Shiomi, J.; Yang, N. Nano-Cross-Junction Effect on Phonon Transport in Silicon Nanowire Cages. *Phys. Rev. B* **2016**, *94*, 165434.
(52) Yang, L.; Yang, N.; Li, B. Extreme low thermal conductivity in nanoscale 3D Si phononic crystal with spherical pores. *Nano Lett.* **2014**, *14*, 1734−1738.
(53) An, M.; Song, Q.; Yu, X.; Meng, H.; Ma, D.; Li, R.; Jin, Z.; Huang, B.; Yang, N. Generalized Two-Temperature Model for Coupled Phonons in Nanosized Graphene. *Nano Lett.* **2017**, *17*, 5805−5810.
(54) Hu, S.; Chen, J.; Yang, N.; Li, B. Thermal Transport in Graphene with Defect and Doping: Phonon Modes Analysis. *Carbon* **2017**, *116*, 139−144.
(55) Hu, S.; Zhang, Z.; Jiang, P.; Chen, J.; Volz, S.; Nomura, M.; Li, B. Randomness-Induced Phonon Localization in Graphene Heat Conduction. *J. Phys. Chem. Lett.* **2018**, *9*, 3959−3968.
(56) Song, Q.; An, M.; Chen, X.; Peng, Z.; Zang, J.; Yang, N. Adjustable Thermal Resistor by Reversibly Folding a Graphene Sheet. *Nanoscale* **2016**, *8*, 14943−14949.
(57) Meng, H.; Ma, D.; Yu, X.; Zhang, L.; Sun, Z.; Yang, N. Thermal conductivity of molybdenum disulfide nanotube from molecular dynamics simulations. *Int. J. Heat Mass Transfer* **2019**, *145*, 118719.
(58) Schelling, P. K.; Phillpot, S. R.; Keblinski, P. Comparison of Atomic-Level Simulation Methods for Computing Thermal Conductivity. *Phys. Rev. B: Condens. Matter Mater. Phys.* **2002**, *65*, 144306.
(59) Liu, J.; Yang, R. Length-Dependent Thermal Conductivity of Single Extended Polymer Chains. *Phys. Rev. B: Condens. Matter Mater. Phys.* **2012**, *86*, 104307.
(60) Wang, X.; Zhang, J.; Chen, Y.; Chan, P. K. Molecular Dynamics Study of Thermal Transport in a Dinaphtho[2,3-B:2′,3′-F]Thieno-[3,2-B]Thiophene (DNTT) Organic Semiconductor. *Nanoscale* **2017**, *9*, 2262−2271.
(61) Zhang, L.; Thingna, J.; He, D.; Wang, J.-S.; Li, B. Nonlinearity Enhanced Interfacial Thermal Conductance and Rectification. *Europhys. Lett.* **2013**, *103*, 64002.
(62) Sääskilahti, K.; Oksanen, J.; Tulkki, J.; Volz, S. Role of Anharmonic Phonon Scattering in the Spectrally Decomposed Thermal Conductance at Planar Interfaces. *Phys. Rev. B: Condens. Matter Mater. Phys.* **2014**, *90*, 134312.
(63) Deng, C.; Yu, X.; Huang, X.; Yang, N. Enhancement of Interfacial Thermal Conductance of SiC by Overlapped Carbon Nanotubes and Intertube Atoms. *International Heat Transfer Conference 16* 2018, Vol. *139*, p 054504.
(64) Zhou, Y.; Xiong, S.; Zhang, X.; Volz, S.; Hu, M. Thermal Transport Crossover from Crystalline to Partial-Crystalline Partial-Liquid State. *Nat. Commun.* **2018**, *9*, 4712.
(65) Shiomi, J.; Maruyama, S. Non-Fourier Heat Conduction in a Single-Walled Carbon Nanotube: Classical Molecular Dynamics Simulations. *Phys. Rev. B: Condens. Matter Mater. Phys.* **2006**, *73*, 205420.
(66) Shiomi, J.; Maruyama, S. Molecular Dynamics of Diffusive-Ballistic Heat Conduction in Single-Walled Carbon Nanotubes. *Jpn. J. Appl. Phys.* **2008**, *47*, 2005−2009.
(67) Ong, Z.-Y.; Pop, E.; Shiomi, J. Reduction of Phonon Lifetimes and Thermal Conductivity of a Carbon Nanotube on Amorphous Silica. *Phys. Rev. B: Condens. Matter Mater. Phys.* **2011**, *84*, 165418.
(68) Wang, X.; Kaviany, M.; Huang, B. Phonon Coupling and Transport in Individual Polyethylene Chains: A Comparison Study with the Bulk Crystal. *Nanoscale* **2017**, *9*, 18022−18031.
(69) Zhang, X.; Bao, H.; Hu, M. Bilateral substrate effect on the thermal conductivity of two-dimensional silicon. *Nanoscale* **2015**, *7*, 6014−6022.

DOI: 10.1021/acs.jpcc.9b09105
J. Phys. Chem. C 2019, 123, 26735−26741